

HUMOF: Human Motion Forecasting in Interactive Social Scenes

Caiyi Sun^{1,2,*}, Yujing Sun^{1,*}, Xiao Han², Zemin Yang²
 Jiawei Liu³, Xinge Zhu⁴, Siu-Ming Yiu¹, Yuexin Ma^{2,†}

¹The University of Hong Kong; ²ShanghaiTech University;

³Sun Yat-sen University; ⁴The Chinese University of Hong Kong
 caiyisun.scy@gmail.com, yjsun@cs.hku.hk, mayuexin@shanghaitech.edu.cn

Abstract

Complex scenes present significant challenges for predicting human behaviour due to the abundance of interaction information, such as human-human and human-environment interactions. These factors complicate the analysis and understanding of human behaviour, thereby increasing the uncertainty in forecasting human motions. Existing motion prediction methods thus struggle in these complex scenarios. In this paper, we propose an effective method for human motion forecasting in interactive scenes. To achieve a comprehensive representation of interactions, we design a hierarchical interaction feature representation so that high-level features capture the overall context of the interactions, while low-level features focus on fine-grained details. Besides, we propose a coarse-to-fine interaction reasoning module that leverages both spatial and frequency perspectives to efficiently utilize hierarchical features, thereby enhancing the accuracy of motion predictions. Our method achieves state-of-the-art performance across four public datasets. **Code will be released when this paper is published.**

1 Introduction

Human motion forecasting is essential across a wide range of applications, including surveillance, healthcare, autonomous driving, and human-robot interaction. The ability to accurately anticipate human behavior in dynamic environments is key to enhancing system safety, operational efficiency, and user experience. However, this task presents significant challenges, including the inherent complexity and variability of human motion, as well as the impact of diverse environmental factors.

In early times, many works predominantly addressed the task of human motion prediction by using simple representations of environmental states. For example, some methods [1; 2; 3; 4; 5; 6; 7; 8; 9] rely solely on past human actions to predict their future motions, while others [10; 11; 12; 13; 14] integrate static scene features into the network all at once. However, these approaches struggle to adapt to real-world applications, where dynamic environmental constraints play a crucial role. Actually, to better predict how humans respond to dynamic environments, it is essential to consider the interaction influence. Some works [15; 16; 17; 18; 19; 20; 21; 22; 23] have started addressing motion prediction in challenging multi-person scenarios, using attention mechanisms to implicitly model the human-human interaction. However, these works overlook the dynamic relationship between humans and the nonhuman environment, which is equally critical for accurate motion forecasting in real scenes.

In fact, real-world environments are inherently complex and dynamic, where existing frequent human-human interactions, e.g., shaking hands, engaging in conversation, as well as human-scene

*Authors contributed equally to this work.

†Corresponding author.

interactions, e.g., sitting on stairs, lying on a bed, as shown in Figure 1. It is important to model all human-related interactions in one framework for more accurate human motion forecasting. Although Mueller et al. [24] made the first attempt to address the problem under this setting, it decouples feature extraction for interacting humans and scenes, fails to fully capture the interaction features, and relies on predefined semantic labels for the scene. As a result, its prediction performance is limited, and it is not practical for real-world applications. The main challenge for forecasting human motion in a realistic and dynamic environment is twofold. Given the vast array of diverse, multi-level interactions between humans and their surroundings, as well as between individuals, *how can we design effective representations to capture these complex interactions?* Moreover, even with well-encoded interaction representations, *how can we leverage them effectively to enhance prediction accuracy?*

In this paper, we have addressed the above two challenges and propose a novel method, named **HUMOF**, for **H**uman **M**otion **F**orecasting in complex scenes. It effectively models human kinematics and dynamics, spatial environment states, temporal information, and the most crucial interaction features, offering significant potential as a world model for human motion. In particular, we introduce a **Hierarchical Interaction Representation** to effectively capture complex and valuable interaction features. The hierarchical representation manifests in several dimensions: (1) It includes both human-human interaction modeling and human-scene interaction modeling; (2) It captures interactions through explicit representations, i.e., interactive distances, and implicitly learns interaction features through the network; (3) It integrates both high-level semantic interaction features and low-level geometric interaction features. Furthermore, to fully utilize the hierarchical representation for enhancing human motion prediction, we design a **Coarse-to-Fine Interaction Reasoning Module**. Specifically, to encourage the model to focus on global environmental understanding while minimizing interference from noisy low-level environmental information and high-frequency details in the earlier stages, and refine fine-grained details in the later stages, we implement the coarse-to-fine mechanism from two perspectives: (1) In spatial perspective, through our coarse-to-fine injection strategy, high-level features are injected into early Transformer layers for semantic understanding of human actions, while low-level features are introduced in later Transformer layers to perceive geometric details; (2) In frequency perspective, our DCT rescaling mechanism suppresses the updating of high-frequency components of human motion in earlier layers, and progressively encourages the model to focus on low-frequency details in later stages. Extensive experimental results demonstrate that our method achieves state-of-the-art performance on four public datasets, and ablation studies show the effectiveness of our detailed designs. Our contributions are summarized as follows:



Figure 1: Real scenes involves complex human-human and human-environment interactions. We propose to predict human motions under such challenging settings, where existing methods struggled.

- We present an effective method for human motion prediction in complex dynamic environments, involving both human-human and human-scene interactions, achieving state-of-the-art performance in various dynamic interactive scenarios.
- We introduce hierarchical interaction feature representation to achieve a comprehensive understanding of environmental dynamics and interactions.
- We propose a coarse-to-fine interaction reasoning module to fully leverage hierarchical interactive features to enhance prediction accuracy.

2 Related Work

Single-Person Human Motion Prediction Early works mainly consider the own kinematic and dynamic influence on future human motions and predict the motion for a single person [1; 2; 3; 4; 5; 6; 7; 8; 9]. Many approaches [25; 26; 27; 28] relied on Recurrent Neural Networks (RNNs) to capture temporal dependencies, overlooking spatial relationships. More recent methods have shifted towards Graph Convolutional Networks [29; 30; 31], Temporal Convolutional Networks [32], and

Transformers [33; 34; 6; 4], aiming to capture complex spatial-temporal relationships. However, these methods primarily concern personal situations to predict future motions, limiting the application in real-world scenarios.

Scene-Aware Human Motion Prediction Recent advancements [10; 11; 12; 13; 14] have started incorporating scene context into human motion prediction tasks. Some approaches [10] represented scenes as 2D images, but struggled when handling occlusions and failed to maintain consistency between local and global motion. GIMO [13] attempted to enhance prediction accuracy by incorporating eye gaze; ContactAware [11] leveraged a contact map to encode human-scene relationships; STAG [12] proposed a three-stage approach that sequentially processes contact points, trajectories, and poses. MutualDistance [14] offered an explicit human-scene interaction model using mutual distance. Although these methods have effectively modeled human-scene interactions, they focus on static scenes, neglecting dynamic social interactions between humans.

Social-Aware Human Motion Prediction Recent studies [35; 36; 15; 16; 17; 37; 18; 19; 20; 21; 22; 38; 23] in multi-person human pose forecasting focus mainly on modeling human interactions in group scenarios. Most recently, Transformers [15; 16; 17; 18; 19; 20; 21; 22; 23] are popular for this task due to their strong learning capabilities: T2P [38] sequentially predicts global trajectory and local pose; IAFormer [23] proposed to learn amplitude-based interactions and prior knowledge. However, methods in this category overlook the importance of scene information. A recent work [24] uses the diffusion model for long-term motion generation considering both static scene and motion of other individuals. However, it only implicitly encodes the scene and other individuals, without explicit modeling of human-to-scene and human-to-human interaction. Additionally, it treats the scene as a set of discrete objects with semantic tags, relying on ground-truth segmentation results, which limits its applicability in real-world scenarios involving raw sensor data.

3 Methodology

The key challenge in forecasting human motion within complex social environments lies in effectively encoding and leveraging the involved human-human and human-scene interactions. Hence, we, on one hand, propose a hierarchical approach to comprehensively encode these representations (Figure 2ab), and on the other hand, present a Coarse-to-Fine Interaction Reasoning Module (Figure 2c) to fully leverage the representations. A more detailed model architecture is in Figure 3.

Problem Definition. The input of our model includes three parts: **1).** A historical motion sequence of the target person $\mathbf{X}^{1:H}$ where $\mathbf{x}_j = \{\mathbf{x}_j^1, \dots, \mathbf{x}_j^H\} \in \mathbb{R}^{H \times 3}$ represents the motion of j -th joint, with each \mathbf{x}_j^t corresponding to the 3D coordinates of a joint at t -th frame; **2).** The scene’s 3D point cloud $\mathcal{S} = \{s_1, \dots, s_N\}$ with N points; And **3).** the historical motion sequence $\mathcal{Y}^{(k)} = [\mathbf{y}_1^{(k)}, \dots, \mathbf{y}_J^{(k)}] \in \mathbb{R}^{J \times H \times 3}$ of the k -th ($k \in [1, K]$) interactive person in the scene, which also consists of J body joints, each with H consecutive poses. Similarly, $\mathbf{y}_j^{(k)} = \{\mathbf{y}_j^{(k)1}, \dots, \mathbf{y}_j^{(k)H}\} \in \mathbb{R}^{H \times 3}$ represents the motion of j -th joint of the k -th interactive person, with each $\mathbf{y}_j^{(k)t}$ corresponding to the 3D coordinates of one of his joint at t -th frame. **Our goal** is to predict the motion $\mathbf{X}^{H+1:H+T}$ of the target person for the future T time steps.

3.1 Motion Encoder

Follow prior works [11; 12; 23; 14], we first pad the sequence $\mathbf{X}^{1:H}$ of length H by repeating the last historical pose \mathbf{X}^H for T additional frames, to make a padded sequence of length $H + T$. For simplicity, we still call the padded sequence \mathbf{X} . Providing that DCT is effective in handling temporal information in human motion prediction [11; 12; 14; 23], and that GCN excels at uncovering spatial

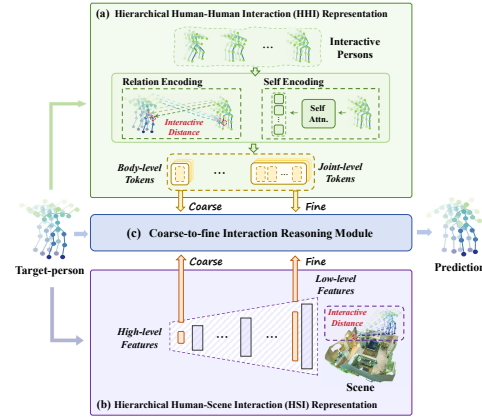


Figure 2: HUMOF Overview.

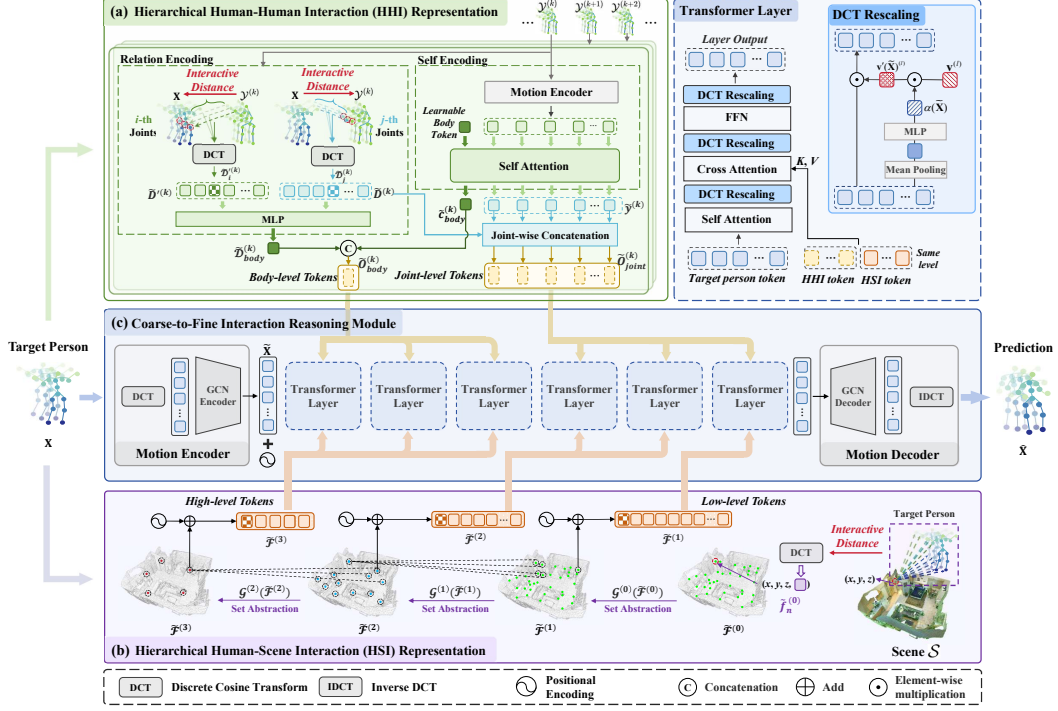


Figure 3: Detailed architecture of HUMOF. Our method takes inputs from three aspects: the past motions of the target person, a 3D point cloud for the scene, and motion sequences of interactive persons. The interactions are comprehensively encoded by (a) Hierarchical Human-Human Interaction Representation and (b) Hierarchical Human-Scene Interaction Representation, respectively. Thereafter, the hierarchical representations are leveraged by (c), a Coarse-to-Fine Interaction Reasoning Module, to predict future motions for the target person. Details of the Interaction-Perceptive Transformer layer in (c) are shown on the top right.

dependencies between human joints [39; 14; 40; 29], we combine a Discrete Cosine Transform layer (DCT) and a Graph Convolutional Network (GCN) [39] to extract both spatial and temporal representations in the motion encoder (Figure 3(c)left). To help the model identify different joints, a learnable position embedding $\mathcal{P} \in \mathbb{R}^{J \times C'}$ is added to each joint. Here $C' = C \times 3$, where $C = 20$ is the number of DCT coefficients and 3 corresponds to the three directions: x , y , and z . Finally, the encoding $\tilde{\mathbf{X}} \in \mathbb{R}^{J \times C'}$ for a person can be formulated as

$$\tilde{\mathbf{X}} = \text{GCN}(\text{DCT}(\mathbf{X})) + \mathcal{P}, \quad (1)$$

which encodes features in the frequency domain for each joint $\tilde{\mathbf{x}}_j$ over the entire motion sequence.

3.2 Hierarchical Interaction Representation

Complex multi-person social scenes involve interactions between humans (Section. 3.2.1), as well as between humans and their environment (Section. 3.2.2). To achieve a comprehensive representation of both human-human and human-scene interactions, we incorporate hierarchical features so that high-level features capture the overall context of the interactions, while low-level features focus on fine-grained details. This multi-level approach ensures a thorough and nuanced understanding of the interactions.

3.2.1 Hierarchical Representation for Human-Human Interaction

Regarding human-level interactions (Figure 3a), when a person engages with others, they are involved in two types of motion: independent motion, such as walking, and interactive motion, such as shaking hands and hugging. Therefore, we introduce a self-encoding submodule (Figure 3a right) to

describe their independent motions and a relation-encoding submodule (Figure 3a left) to model their interdependencies.

Self Encoding. For each interactive person, we encode their motion sequence independently, capturing semantic information specific to his motion, as shown in Figure 3(a) right. This self-encoding step enables each person’s motion to contribute meaningful social cues. Specifically, the motion sequence $\mathcal{Y}^{(k)}$ of k_{th} interactive person is first processed through a motion encoder as described in Section 3.1, obtaining **joint-level features** in the frequency domain $\tilde{\mathcal{Y}}^{(k)} = \{\tilde{\mathbf{y}}_1^{(k)}, \dots, \tilde{\mathbf{y}}_J^{(k)}\} \in \mathbb{R}^{J \times C'}$. Then a two-layer Transformer processes a learnable body-level feature $\tilde{c}_{body}^{(k)}$ together with the joint-level feature $\tilde{\mathcal{Y}}^{(k)}$. Note that **body-level feature** $\tilde{c}_{body}^{(k)}$ contains the information from all joints after being passed by the Transformer, serving as the body-level self encoding. While the updated joint tokens $\tilde{\mathcal{Y}}^{(k)} = \{\tilde{\mathbf{y}}_1^{(k)}, \dots, \tilde{\mathbf{y}}_J^{(k)}\}$ constitute the joint-level self encoding.

Relation Encoding. We observe that despite of the various types of interactions, different interactions always lead to distinct distance patterns. Therefore, it is effective and efficient to model interactions with "distances". Hence we model the interactions explicitly to capture their dependencies via defining interactive distances as shown in Figure 3(a) left. First, for the j_{th} joint of the k_{th} interactive person, we calculate the interactive distance between this joint and the closest joint of the target person for each of the H frames as the **joint-level relation encoding**. Specifically, at t_{th} frame, the joint-level interactive distance $\mathbf{D}_j^{(k)t}$ is computed as:

$$\mathbf{D}_j^{(k)t} = \phi\left(\min_{i \in [1, J]} \|\mathbf{y}_j^{(k)t} - \mathbf{x}_i^t\|_2^2\right), \quad (2)$$

where $\phi(\cdot)$ is a mapping function such that closer joints have higher values than more distant ones. Then, we convert the time series of interactive distances $\{\mathbf{D}_j^{(k)1}, \dots, \mathbf{D}_j^{(k)H}\}$ into frequency domain via DCT to get the joint-level relationship encoding $\tilde{\mathbf{D}}_j^{(k)} \in \mathbb{R}^C$. Second, for the i_{th} joint of the target person, we similarly calculate its joint-level relationship encoding with the k_{th} interactive person, denoted as $\tilde{\mathbf{D}}_i'^{(k)}$. Thereafter, we obtained the **body-level relation encoding** $\tilde{\mathbf{D}}_{body}^{(k)} = \text{MLP}(\text{concat}(\tilde{\mathbf{D}}_1^{(k)}, \dots, \tilde{\mathbf{D}}_J^{(k)}, \tilde{\mathbf{D}}_1'^{(k)}, \dots, \tilde{\mathbf{D}}_J'^{(k)}))$.

Human-Human Interaction Tokens. Finally, we concatenate the Self Encoding and Relation Encoding on their respective levels to obtain the Human-Human Interaction (HHI) token. To be clear, the k_{th} interactive person’s body-level HHI token is $\tilde{O}_{body}^{(k)} = \text{concat}(\tilde{c}_{body}^{(k)}, \tilde{\mathbf{D}}_{body}^{(k)})$, and joint-level HHI token is $\tilde{O}_{joint}^{(k)} = \{\tilde{o}_1^{(k)}, \dots, \tilde{o}_J^{(k)}\}$, where $\tilde{o}_j^{(k)} = \text{concat}(\tilde{\mathbf{y}}_j^{(k)}, \tilde{\mathbf{D}}_j^{(k)})$.

3.2.2 Hierarchical Representation for Human-Scene Interaction

Considering the vast number of points in the 3D point cloud of a scene, it is impractical and inefficient to enumerate the target person’s interactions with every point. Recalling that a centre point is frequently used to represent its neighbouring points as an approximation in geometric processing, we hope to progressively approximate neighbouring points through central points, reducing the total number of points while retaining essential scene information. In this way, we can construct different levels of point approximations with a gradually decreasing number of points, ensuring to maintain rich interaction features across different spatial scales. Meanwhile, noting that most raw 3D scene point clouds lack object-level annotations, our method does not rely on predefined semantic labels as required by SAST [24].

As illustrated in Figure 3(b), to obtain hierarchical point approximations, we employ a series of set abstraction layers from PointNet++ [41], denoted as $\{\mathcal{G}^{(0)}, \dots, \mathcal{G}^{(b)}\}$, $b \in [0, 3]$. Each set abstraction operation processes and refines the point set to create a new set with fewer points, preserving efficiency and structure within the point cloud.

Notice that the set abstraction layer $\mathcal{G}^{(0)}$ takes an interactive feature matrix $\tilde{\mathcal{F}}^{(0)} = \{\tilde{f}_1^{(0)}, \dots, \tilde{f}_{N^{(0)}}^{(0)}\}$ as input, where the interactive feature $\tilde{f}_n^{(0)}$ of a point s_n is computed as a collection of interactive distances in the frequency domain. Specifically, for a point s_n and a joint \mathbf{x}_j , we firstly calculate their interactive distance in each frame, constituting a time series m_j :

$$m_j = \{\phi(\|s_n - \mathbf{x}_j^1\|_2^2), \dots, \phi(\|s_n - \mathbf{x}_j^H\|_2^2)\} \in \mathbb{R}^H, \quad (3)$$

where $\phi(\cdot)$ is a mapping function that closer scene points have higher values than more distant ones [11]. Next, we convert m_j into frequency domain and obtain $\tilde{m}_j \in \mathbb{R}^{C'}$. Finally, we concatenate \tilde{m}_j from all joints, along with the coordinates of the scene point s_n , forming s_n 's interactive feature $\tilde{f}_n^{(0)} \in \mathbb{R}^{J \times C' + 3}$.

Such a feature matrix $\tilde{\mathcal{F}}^{(b)}$ is iteratively computed across subsequent set abstraction layers (Figure 3(b)), where $\tilde{\mathcal{F}}^{(b)} = \mathcal{G}^{(b-1)}(\tilde{\mathcal{F}}^{(b-1)})$. To further enhance the positional information, we add a position encoding derived from 3D spatial coordinates of each point to the corresponding feature at each abstraction level $b \in [1, 3]$. Finally, $\tilde{\mathcal{F}}^{(b)}$ serves as the Human-Scene Interaction (HSI) tokens.

3.3 Coarse-to-Fine Interaction Reasoning Module

Accurate human motion prediction requires capturing kinetics and dynamics, involving inherent correlations among joints, across the temporal dimension, and with the surrounding environment. To simultaneously leverage these three types of correlations, we present a coarse-to-fine interaction reasoning module. We take the target person's representation $\tilde{\mathbf{X}}$ and all the interaction features in the frequency domain including human-to-human interactions (HHI) tokens (\tilde{O}_{body} and \tilde{O}_{joint}) and human-to-scene interactions (HSI) tokens $\tilde{\mathcal{F}}^{(b)}$ as input, the model reasons about the motion of the target person through all interaction-perceptive Transformer layers using a coarse-to-fine strategy.

3.3.1 Coarse-to-Fine Injection Strategy

With the obtained hierarchical representations for interactions—both between human and human (Section 3.2.1) and between humans and scenes (Section 3.2.2)—we establish a strategy to fully leverage this information.

Different from crudely injecting features from multiple levels of the hierarchical representation into each interaction layer of the model, we sequentially inject hierarchical interaction features in a coarse-to-fine manner. We assign high-level features to early layers and progressively incorporate low-level features at deeper layers, as shown in Figure 3(c). For example, at the first layer, high-level HSI tokens $\tilde{\mathcal{F}}^{(3)}$ and HHI tokens \tilde{O}_{body} are concatenated along token dimension and injected, totaling $N^{(3)} + K$ interaction tokens. At the last layer, we inject low-level HSI tokens $\tilde{\mathcal{F}}^{(1)}$ and HHI tokens \tilde{O}_{joint} , totaling $N^{(1)} + K \times J$ tokens. This strategy allows the model to begin with a global understanding of high-level semantics and gradually narrow its focus to local geometry, improving prediction accuracy.

3.3.2 Interaction-Perceptive Transformer Layer

As depicted in the upper right of Figure 3, our Transformer layer begins with processing the target person's joint tokens $\tilde{\mathbf{x}}_j^{(l)}$ via a self-attention (SA) designed to capture long-range dependencies among joints. To incorporate interactions, we employ a cross-attention (CA) where joint tokens $\tilde{\mathbf{x}}_j^{(l)}$ serve as queries, while interaction tokens act as keys and values. A feed forward network (FFN) [42] follows CA to enhance joint tokens. More importantly, to better align with our coarse-to-fine strategy, an adaptive DCT rescaling mechanism is performed on $\tilde{\mathbf{x}}_j^{(l)}$ after each SA, CA and FFN.

Adaptive DCT Rescaling Mechanism. Recall that our coarse-to-fine injection strategy focuses on capturing coarse-level human motions in the early stages, it would be helpful if we could control the influence of finer details. Observing that each primary joint token is constructed from the DCT coefficients of joint motion, with each channel corresponding to a specific DCT coefficient, we introduce a learnable DCT rescaling mechanism from the frequency domain to suppress high-frequency details. This mechanism further supports our coarse-to-fine strategy by regulating the impact of high-frequency details and noise in the Transformer layer l through the rescaling vector $\mathbf{v}'(\tilde{\mathbf{X}})^{(l)} \in \mathbb{R}^{C'}$, which is applied on joint tokens $\tilde{\mathbf{x}}_j^{(l)}$ after each SA, CA, and FFN in an element-wise

multiplication manner, formulated as $\tilde{\mathbf{x}}_j^{(l)} \leftarrow \tilde{\mathbf{x}}_j^{(l)} \odot \mathbf{v}'(\tilde{\mathbf{X}})^{(l)}$ where

$$\begin{aligned}\mathbf{v}'(\tilde{\mathbf{X}})^{(l)} &= \mathbf{v}^{(l)} \odot \boldsymbol{\alpha}(\tilde{\mathbf{X}}) \\ \boldsymbol{\alpha}(\tilde{\mathbf{X}}) &= \text{MLP}\left(\frac{\sum_{j=1}^J \tilde{\mathbf{x}}_j^{(l)}}{J}\right)\end{aligned}\tag{4}$$

Here, \odot is element-wise multiplication, and $\mathbf{v}^{(l)}$ is a pre-defined rescaling vector shared across all joint tokens. We design $\mathbf{v}^{(l)}$ such that values are close to 1.0 for low-frequency components and progressively decrease for higher frequencies in early layers, effectively suppressing high-frequency components. The suppression is most prominent in the first layer ($l = 1$) and gradually weakens in deeper layers, with the rescaling vector eventually having all values equal to 1.0 in the last layer ($l = 6$). Moreover, for that different types of action may have varied optimal rescaling, a shared rescaling $\mathbf{v}^{(l)}$ applied uniformly across all input samples is inadequate. We thus further include a sample-adaptive vector $\boldsymbol{\alpha}(\tilde{\mathbf{X}})$ to capture such variations, which is computed by applying average pooling across all J joint tokens, followed by a MLP to acquire sample-specific information.

3.4 Motion Decoder and Loss

As shown in Figure 3(c) right, the updated joint tokens $\tilde{\mathbf{X}}^{(6)}$ from the 6_{th} Transformer layer is passed into a GCN decoder and Inverse Discrete Cosine Transform (IDCT) [39] to get predicted motion sequence $\hat{\mathbf{X}}$, which is formulated by $\hat{\mathbf{X}} = \text{IDCT}(\text{GCN}(\tilde{\mathbf{X}}^{(6)})) \in \mathbb{R}^{J \times (H+T) \times 3}$.

Loss is computed as $\ell = \ell_{\text{path}} + \ell_{\text{pose}}$. The global path loss ℓ_{path} local and pose loss ℓ_{pose} are defined as

$$\begin{aligned}\ell_{\text{path}} &= \frac{1}{T} \sum_{t=H+1}^{H+T} \left\| \mathbf{X}_{\text{root}}^t - \hat{\mathbf{X}}_{\text{root}}^t \right\|_2^2 \\ \ell_{\text{local}} &= \frac{1}{T(J-1)} \sum_{t=H+1}^{H+T} \sum_{j=1}^{J-1} \left\| \mathbf{X}_{\text{local},j}^t - \hat{\mathbf{X}}_{\text{local},j}^t \right\|_2^2.\end{aligned}\tag{5}$$

Here, $\mathbf{X}_{\text{root}}^t \in \mathbb{R}^3$ and $\hat{\mathbf{X}}_{\text{root}}^t \in \mathbb{R}^3$ are the ground-truth and predicted global path of the root joint at time t . $\mathbf{X}_{\text{local},j}^t \in \mathbb{R}^3$ and $\hat{\mathbf{X}}_{\text{local},j}^t \in \mathbb{R}^3$ are the ground-truth and predicted local pose of the j^{th} non-root joint at time t .

4 Experiments

4.1 Setups

Implementation Details. We build our network on PyTorch 1.12.0 and CUDA 12.4. We follow previous work [11] to use the Adam optimizer with a linear learning rate schedule from 0.0005 to 0. The initial learning rate is 0.0005. Models are trained over 80 epochs. For each motion sequence, we crop the 3D scene to a region that is within 2.5 meters of the root joint of the last observed pose, and the root joint is used as the origin of the cropped scene, following prior works [11; 12]. Then we obtain $\mathcal{S} \in \mathbb{R}^{N \times 3}$ by randomly sampling $N = 1000$ points in the cropped scene. We use $H = 30$ motion frames to predict $T = 60$ future steps for datasets HIK [43], HOI-M³ [44] and GTA-IM [10], $H = 15$ and $T = 30$ for HUMANISE [45]. The mapping function $\phi(\cdot)$ is defined similarly as in [11], $\phi(\cdot) : d \rightarrow e^{-\frac{d^2}{2\sigma^2}}$.

Datasets. We conduct experiments on 2 datasets with interactive social scenes, as well as on 2 datasets with human-scene interaction scenes. **A. Datasets with Interactive Social Scenes.** 1) **HIK** [43] is a multi-person interaction datasets in real kitchen environments. We follow the dataset split used in [43; 24], using the recordings A-C as training data and evaluating on the recording D. 2) **HOI-M³** [44] captures a rich collection of interactions involving multiple humans and objects across 46 diverse scenes in the real world. We randomly allocate 1/5 of these scenes for the test set and utilize the remaining for training. For both datasets, we filter out sequences with few social interactions and human movements, and retain those with rich interactions and significant motion displacement. **B. Datasets with Human-Scene Interaction Scenes.** 1) **GTA-IM** [10] is a synthetic human-scene

Dataset	Method	Path Error (mm)					Pose Error (mm)				
		0.5s	1.0s	1.5s	2.0s	mean	0.5s	1.0s	1.5s	2.0s	mean
HIK [43]	ContAware [11]	138.3	251.3	352.4	430.8	239.3	87.8	117.1	136.1	147.8	106.8
	GIMO [13]	143.0	259.7	384.2	487.3	258.6	85.5	121.6	142.0	153.0	109.3
	STAG [12]	124.7	245.4	352.4	479.2	239.7	81.7	110.9	132.5	140.9	100.6
	MutualDistance [14]	128.7	253.2	372.5	479.2	246.0	82.9	117.2	138.5	148.2	105.9
	T2P [38]	88.6	199.6	318.8	447.1	208.7	74.2	108.6	127.5	142.6	96.9
	IAFormer [23]	83.9	195.0	311.1	434.9	200.1	71.5	106.5	125.9	137.7	95.0
	SAST [24]	86.7	187.4	284.9	398.1	189.0	72.3	101.4	118.0	128.6	93.2
	Ours	78.8	177.4	278.8	388.4	180.7	71.2	100.6	116.9	127.1	90.2
HOI-M ³ [44]	ContAware [11]	125.6	239.9	285.4	432.9	236.9	106.2	152.8	174.3	197.1	137.5
	GIMO [13]	131.4	247.7	300.9	454.4	255.2	107.9	155.9	182.6	207.1	141.0
	STAG [12]	128.1	234.4	289.5	438.1	239.7	102.5	145.0	167.1	185.6	131.2
	MutualDistance [14]	83.6	169.7	278.8	402.8	189.9	94.4	137.1	158.2	181.3	125.3
	T2P [38]	74.2	168.8	296.9	429.2	194.1	88.0	135.8	160.9	183.2	124.6
	IAFormer [23]	69.0	166.6	290.1	423.5	186.3	86.1	135.0	165.9	180.7	121.6
	SAST [24]	75.0	166.2	280.4	403.9	184.8	89.2	133.8	167.0	182.9	122.3
	Ours	67.1	156.6	268.4	393.1	174.6	86.3	129.6	155.0	172.1	117.9

Table 1: Comparisons on datasets with interactive social scenes. We compare with scene-aware methods [11; 13; 12; 14], social-aware method [38; 23] and social-scene-aware method SAST [24].

interaction dataset, comprising 3D human motions for 50 distinct characters across 7 diverse scenes. All methods share the same dataset setting as [11; 12; 14]. 2) **HUMANISE** [45] is a synthetic human-scene interaction dataset. All methods adopt the dataset setting used in MutualDistance [14] which ensures motions in the test set are entirely unseen during training. The test set scenes are further divided into seen and unseen scenes, with about 6,000 sub-sequences for testing.

Method	Path Error (mm)					Pose Error (mm)				
	0.5s	1.0s	1.5s	2.0s	mean	0.5s	1.0s	1.5s	2.0s	mean
ContAware [11] *	44.5	82.6	125.6	182.9	87.1	40.1	54.1	65.2	77.2	51.8
GIMO [13]*	52.7	97.8	160.6	241.7	110.3	47.9	60.7	71.1	82.7	59.9
STAG [12]*	43.2	79.8	119.9	176.4	83.4	35.4	48.7	59.8	73.5	47.0
SAST [24]	41.0	77.4	123.1	181.8	85.2	28.2	41.0	53.6	66.8	41.5
MutualDistance [14]*	34.4	65.9	104.0	155.6	72.0	31.0	46.8	58.9	70.7	44.6
Ours	29.4	55.9	91.7	139.2	62.9	27.0	40.3	50.7	61.5	38.7

Table 2: Comparisons on dataset with static scenes GTA-IM [10]. Results with * are from [14].

Method	Seen Scenes						Unseen Scenes					
	Path Error (mm)			Pose Error (mm)			Path Error (mm)			Pose Error (mm)		
	0.5s	1.0s	mean	0.5s	1.0s	mean	0.5s	1.0s	mean	0.5s	1.0s	mean
ContAware [11] *	52.8	121.1	57.8	97.6	141.4	92.9	53.1	124.0	58.7	94.0	139.1	90.3
GIMO [13] *	70.1	129.2	72.0	141.4	150.3	140.2	77.7	144.0	80.2	146.3	159.4	146.5
STAG [12] *	55.2	124.6	60.7	88.3	131.4	83.0	57.0	131.5	63.2	89.9	137.7	85.6
SAST [24]	56.2	122.4	62.1	86.0	111.6	80.8	57.2	129.1	63.7	90.6	124.7	86.7
MutualDistance [14] *	41.5	93.5	45.6	83.7	130.9	80.0	46.7	100.2	50.1	84.3	131.8	80.6
Ours	36.9	87.4	41.7	69.0	102.0	64.1	39.5	88.1	43.4	69.8	109.3	66.2

Table 3: Comparisons on dataset with static scenes HUMANISE [45]. Results with * are from [14].

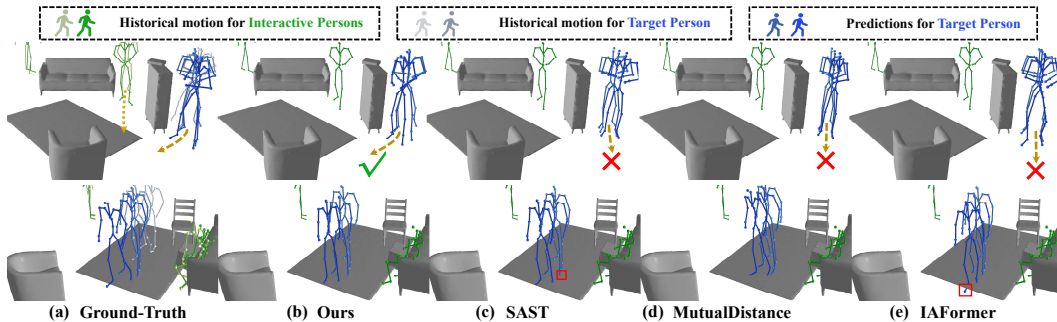


Figure 4: Visualization of motion prediction results on interactive social scenes in HOI-M³.

Baselines. We compare our method with three types of human motion prediction methods: **A. Scene-Aware Methods:** ContactAware [11], GIMO [13], STAG [12], and MutualDistance [14]. To evaluate them on dynamic social datasets, we introduce the multi-person context by concatenating all persons’ information to the original input of their motion decoder. **B. Social-Aware Methods:**

T2P [38] and IAFormer [23], which are SOTAs for multi-person motion predictions. Since they are highly dedicated to pure multi-person input, we introduce the human-scene-interaction features generated by our HUMOF. **C. Social-Scene-Aware Methods:** SAST [24], which is a diffusion-based method for long-term motion generation under the guidance of objects in the scene and motion of other individuals. As it requires instance segmentation of the scene as input, we provide it with the ground-truth segmentations, except on GTA-IM, where we use the segmentation predicted by [46] due to the absence of ground truth.

Metrics. Following prior works [11; 12; 14], we evaluate all methods using path error and pose error, which are computed in the same way as ℓ_{path} and ℓ_{pose} defined in Eq. 5.

4.2 Comparisons and Discussions

Evaluations on Interactive Social Scenes We first quantitatively evaluate our approach on two real-world datasets with dynamic social scenes, HIK [43] and HOI-M³ [44]. As demonstrated in Table 1, our approach achieves outstanding superior performance to all other methods in three categories, highlighting our strong capability in forecasting human motion in real scenarios with complex human-human and human-scene dynamics. Visual comparisons on dynamic scenes in HOI-M³ are shown in Figure 4. In the first example, the target person exhibits a tendency to turn toward the interactive person. Only our method captures this intent and correctly predicts the direction. In the second example, SAST and IAFormer mistakenly infer some poses to be underneath the floor (marked in red boxes). In contrast, our result shows the best physical plausibility and provides the most accurate path and pose prediction.

Evaluations on Human-Scene Interaction Scenes are shown in Table 3 and Table 2. We demonstrate significantly superior performance over SOTA scene-aware methods [11; 12; 14; 13] on both the HUMANISE [45] and GTA-IM [10] datasets. Meanwhile, our method also greatly outperforms the social-scene-aware method SAST [24]. Note that we do not rely on ground truth instance segmentation, which is required by SAST.

Joint Multi-Person Inference Our method is readily scalable to joint multi-person motion forecasting by treating each individual as a separate target in a data sample and then inferring the batch (batch size = $1 + K$). A visual result is shown in Figure 5.

Runtime Analysis Our model takes similar or shorter time to perform inference than other methods. Specifically, our model has 9.6M parameters and achieves an inference time of 43ms on HOI-M³. See Appendix for more detailed comparisons with baselines.

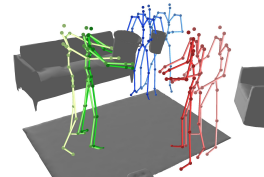


Figure 5: Joint forecasting.

More qualitative and visual results are provided in the Supplementary Video and Appendix.

4.3 Ablation Studies on the HOI-M3 Dataset

Hierarchical Interaction Representation. Table 4(a) shows the effectiveness of our human-to-scene and human-to-human (including self-encoding and relation-encoding) interaction representations. Results indicate a decline in our motion prediction performance when any of these modules are removed, underscoring their individual contributions.

Coarse-to-Fine Interaction Feature Injection. We assess the effectiveness of the coarse-to-fine interaction feature injection strategy in Table 4(b). The experiment shows that multi-level interaction feature injection outperforms single-level approaches (coarse-only and fine-only). But our coarse-to-fine strategy utilizes multi-level features in a more effective way and further boosts the performance.

Adaptive DCT Rescaling. Table 4(c) validates the effectiveness of the adaptive DCT rescaling mechanism. By suppressing high-frequency updates of joint motion in early stages to encourage the focus on coarse and low-frequency updates, the shared static rescaling vector $\mathbf{v}^{(l)}$ itself improves prediction accuracy. Besides, the performance is further enhanced after combining the sample-adaptive vector $\alpha(\tilde{\mathbf{X}})$, as it allows the frequency rescalings to adapt to different input samples.

(a) Hierarchical Representations									(b) Injection Strategy						(c) Adaptive DCT Rescaling											
HSI	HHI		Path Error (mm)			Pose Error (mm)			Injection strategy			Path Error (mm)			Pose Error (mm)			DCT rescaling			Path Error (mm)			Pose Error (mm)		
	Self	Relation	1.0s	2.0s	mean	1.0s	2.0s	mean				1.0s	2.0s	mean	1.0s	2.0s	mean				$\sqrt{()}$	$\alpha(\bar{X})$	1.0s	2.0s	mean	1.0s
	✗	✗	✓	✓	✓	167.0	426.8	187.6	134.7	181.8	123.2															
	✗	✓	✓	✓	✓	164.1	415.7	183.7	133.2	175.5	120.9															
	✓	✗	✗	✗	✗	163.0	414.0	182.9	132.8	179.2	121.4															
	✓	✓	✗	✗	✗	160.0	402.7	178.4	132.0	175.0	120.0															
	✓	✗	✓	✓	✓	158.2	401.0	177.0	131.4	175.6	119.9															
	✓	✓	✓	✓	✓	156.6	393.1	174.6	129.6	172.1	117.9															

Table 4: Ablations studies.

5 Conclusion

In conclusion, we present an effective approach for human motion forecasting in interactive environments. By representing hierarchical interactive features and employing the coarse-to-fine interaction reasoning module, our method achieves state-of-the-art performance across four public datasets, demonstrating the potential to construct a world model for human motion. This approach holds significant promise for real-world applications, such as enhancing closed-loop simulations for autonomous driving and improving the understanding and interaction capabilities of robots.

References

- [1] Wanying Zhang, Shen Zhao, Fanyang Meng, Songtao Wu, and Mengyuan Liu. Dynamic compositional graph convolutional network for efficient composite human motion prediction. In *Proceedings of the 31st ACM International Conference on Multimedia*, pages 2856–2864, 2023.
- [2] Chenxin Xu, Robby T Tan, Yuhong Tan, Siheng Chen, Yu Guang Wang, Xinchao Wang, and Yanfeng Wang. Eqmotion: Equivariant multi-agent motion prediction with invariant interaction reasoning. In *Proceedings of the IEEE/CVF Conference on Computer Vision and Pattern Recognition*, pages 1410–1420, 2023.
- [3] Tiezheng Ma, Yongwei Nie, Chengjiang Long, Qing Zhang, and Guiqing Li. Progressively generating better initial guesses towards next stages for high-quality human motion prediction. In *Proceedings of the IEEE/CVF Conference on Computer Vision and Pattern Recognition*, pages 6437–6446, 2022.
- [4] Chenxin Xu, Robby T Tan, Yuhong Tan, Siheng Chen, Xinchao Wang, and Yanfeng Wang. Auxiliary tasks benefit 3d skeleton-based human motion prediction. In *Proceedings of the IEEE/CVF International Conference on Computer Vision*, pages 9509–9520, 2023.
- [5] Xuehao Gao, Shaoyi Du, Yang Wu, and Yang Yang. Decompose more and aggregate better: Two closer looks at frequency representation learning for human motion prediction. In *Proceedings of the IEEE/CVF conference on computer vision and pattern recognition*, pages 6451–6460, 2023.
- [6] Emre Aksan, Manuel Kaufmann, Peng Cao, and Otmar Hilliges. A spatio-temporal transformer for 3d human motion prediction. In *2021 International Conference on 3D Vision (3DV)*, pages 565–574. IEEE, 2021.
- [7] Zhihao Wang, Yulin Zhou, Ningyu Zhang, Xiaosong Yang, Jun Xiao, and Zhao Wang. Existence is chaos: Enhancing 3d human motion prediction with uncertainty consideration. In *Proceedings of the AAAI Conference on Artificial Intelligence*, volume 38, pages 5841–5849, 2024.
- [8] Pengxiang Su, Zhenguang Liu, Shuang Wu, Lei Zhu, Yifang Yin, and Xuanjing Shen. Motion prediction via joint dependency modeling in phase space. In *Proceedings of the 29th ACM International Conference on Multimedia*, pages 713–721, 2021.
- [9] Jianwei Tang, Jieming Wang, and Jian-Fang Hu. Predicting human poses via recurrent attention network. *Visual Intelligence*, 1(1):18, 2023.
- [10] Zhe Cao, Hang Gao, Karttikeya Mangalam, Qi-Zhi Cai, Minh Vo, and Jitendra Malik. Long-term human motion prediction with scene context. In *ECCV*, pages 387–404. Springer, 2020.
- [11] Wei Mao, Richard I Hartley, Mathieu Salzmann, et al. Contact-aware human motion forecasting. *Advances in Neural Information Processing Systems*, 35:7356–7367, 2022.
- [12] Luca Scofano, Alessio Sampieri, Elisabeth Schiele, Edoardo De Matteis, Laura Leal-Taixé, and Fabio Galasso. Staged contact-aware global human motion forecasting. In *BMVC*, 2023.

- [13] Yang Zheng, Yanchao Yang, Kaichun Mo, Jiaman Li, Tao Yu, Yebin Liu, C Karen Liu, and Leonidas J Guibas. Gimo: Gaze-informed human motion prediction in context. In *European Conference on Computer Vision*, pages 676–694. Springer, 2022.
- [14] Chaoyue Xing and etc. Scene-aware human motion forecasting via mutual distance prediction. In *ECCV*, 2025.
- [15] Jiashun Wang, Huazhe Xu, Medhini Narasimhan, and Xiaolong Wang. Multi-person 3d motion prediction with multi-range transformers. *Advances in Neural Information Processing Systems*, 34:6036–6049, 2021.
- [16] Wen Guo, Xiaoyu Bie, Xavier Alameda-Pineda, and Francesc Moreno-Noguer. Multi-person extreme motion prediction. In *Proceedings of the IEEE/CVF conference on computer vision and pattern recognition*, pages 13053–13064, 2022.
- [17] Edward Vendrow, Satyajit Kumar, Ehsan Adeli, and Hamid Rezatofighi. Somoformer: Multi-person pose forecasting with transformers. *arXiv preprint arXiv:2208.14023*, 2022.
- [18] Saeed Saadatnejad, Yang Gao, Kaouther Messaoud, and Alexandre Alahi. Social-transmotion: Promptable human trajectory prediction. In *International Conference on Learning Representations (ICLR)*, 2024.
- [19] Xuehao Gao, Yang Yang, Yang Wu, Shaoyi Du, and Guo-Jun Qi. Multi-condition latent diffusion network for scene-aware neural human motion prediction. *IEEE Transactions on Image Processing*, 2024.
- [20] Yang Gao, Po-Chien Luan, and Alexandre Alahi. Multi-transmotion: Pre-trained model for human motion prediction. *arXiv preprint arXiv:2411.02673*, 2024.
- [21] Qingyao Xu, Weibo Mao, Jingze Gong, Chenxin Xu, Siheng Chen, Weidi Xie, Ya Zhang, and Yanfeng Wang. Joint-relation transformer for multi-person motion prediction. In *Proceedings of the IEEE/CVF International Conference on Computer Vision*, pages 9816–9826, 2023.
- [22] Xiaogang Peng, Siyuan Mao, and Zizhao Wu. Trajectory-aware body interaction transformer for multi-person pose forecasting. In *Proceedings of the IEEE/CVF conference on computer vision and pattern recognition*, pages 17121–17130, 2023.
- [23] Peng Xiao, Yi Xie, Xuemiao Xu, Weihong Chen, and Huaidong Zhang. Multi-person pose forecasting with individual interaction perceptron and prior learning. In *European Conference on Computer Vision*, pages 402–419. Springer, 2025.
- [24] Felix B Mueller, Julian Tanke, and Juergen Gall. Massively multi-person 3d human motion forecasting with scene context. *arXiv preprint arXiv:2409.12189*, 2024.
- [25] Katerina Fragkiadaki, Sergey Levine, Panna Felsen, and Jitendra Malik. Recurrent network models for human dynamics. In *ICCV*, pages 4346–4354, 2015.
- [26] Ashesh Jain, Amir R Zamir, Silvio Savarese, and Ashutosh Saxena. Structural-rnn: Deep learning on spatio-temporal graphs. In *Proceedings of the IEEE conference on computer vision and pattern recognition*, pages 5308–5317, 2016.
- [27] Julieta Martinez, Michael J Black, and Javier Romero. On human motion prediction using recurrent neural networks. In *Proceedings of the IEEE conference on computer vision and pattern recognition*, pages 2891–2900, 2017.
- [28] Zhenguang Liu, Shuang Wu, Shuyuan Jin, Shouling Ji, Qi Liu, Shijian Lu, and Li Cheng. Investigating pose representations and motion contexts modeling for 3d motion prediction. *IEEE transactions on pattern analysis and machine intelligence*, 45(1):681–697, 2022.
- [29] Maosen Li, Siheng Chen, Zijing Zhang, Lingxi Xie, Qi Tian, and Ya Zhang. Skeleton-parted graph scattering networks for 3d human motion prediction. In *European conference on computer vision*, pages 18–36. Springer, 2022.
- [30] Ming Chen, Zhewei Wei, Zengfeng Huang, Bolin Ding, and Yaliang Li. Simple and deep graph convolutional networks. In *International conference on machine learning*, pages 1725–1735. PMLR, 2020.
- [31] Lingwei Dang, Yongwei Nie, Chengjiang Long, Qing Zhang, and Guiqing Li. Msr-gcn: Multi-scale residual graph convolution networks for human motion prediction. In *Proceedings of the IEEE/CVF international conference on computer vision*, pages 11467–11476, 2021.
- [32] Theodoros Sofianos, Alessio Sampieri, Luca Franco, and Fabio Galasso. Space-time-separable graph convolutional network for pose forecasting. In *Proceedings of the IEEE/CVF International Conference on Computer Vision*, pages 11209–11218, 2021.

- [33] Wei Mao, Miaomiao Liu, and Mathieu Salzmann. History repeats itself: Human motion prediction via motion attention. In *ECCV*, pages 474–489. Springer, 2020.
- [34] Yujun Cai, Lin Huang, Yiwei Wang, Tat-Jen Cham, Jianfei Cai, Junsong Yuan, Jun Liu, Xu Yang, Yiheng Zhu, Xiaohui Shen, et al. Learning progressive joint propagation for human motion prediction. In *ECCV*, pages 226–242. Springer, 2020.
- [35] Vida Adeli, Ehsan Adeli, Ian Reid, Juan Carlos Niebles, and Hamid Rezaatoughi. Socially and contextually aware human motion and pose forecasting. *IEEE Robotics and Automation Letters*, 5(4):6033–6040, 2020.
- [36] Vida Adeli, Mahsa Ehsanpour, Ian Reid, Juan Carlos Niebles, Silvio Savarese, Ehsan Adeli, and Hamid Rezaatoughi. Tripod: Human trajectory and pose dynamics forecasting in the wild. In *Proceedings of the IEEE/CVF International Conference on Computer Vision*, pages 13390–13400, 2021.
- [37] Julian Tanke, Linguang Zhang, Amy Zhao, Chengcheng Tang, Yujun Cai, Lezi Wang, Po-Chen Wu, Juergen Gall, and Cem Keskin. Social diffusion: Long-term multiple human motion anticipation. In *Proceedings of the IEEE/CVF International Conference on Computer Vision*, pages 9601–9611, 2023.
- [38] Jaewoo Jeong and etc. Multi-agent long-term 3d human pose forecasting via interaction-aware trajectory conditioning. In *CVPR*, 2024.
- [39] Wei Mao, Miaomiao Liu, Mathieu Salzmann, and Hongdong Li. Learning trajectory dependencies for human motion prediction. In *ICCV*, pages 9489–9497, 2019.
- [40] Maosen Li, Siheng Chen, Yangheng Zhao, Ya Zhang, Yanfeng Wang, and Qi Tian. Dynamic multiscale graph neural networks for 3d skeleton based human motion prediction. In *Proceedings of the IEEE/CVF conference on computer vision and pattern recognition*, pages 214–223, 2020.
- [41] Charles Ruizhongtai Qi, Li Yi, Hao Su, and Leonidas J Guibas. Pointnet++: Deep hierarchical feature learning on point sets in a metric space. *Advances in neural information processing systems*, 30, 2017.
- [42] Ashish Vaswani, Noam Shazeer, Niki Parmar, Jakob Uszkoreit, Llion Jones, Aidan N Gomez, Łukasz Kaiser, and Illia Polosukhin. Attention is all you need. In *NeurIPS*, pages 5998–6008, 2017.
- [43] Julian Tanke, Oh-Hun Kwon, Felix B Mueller, Andreas Doering, and Juergen Gall. Humans in kitchens: a dataset for multi-person human motion forecasting with scene context. *Advances in Neural Information Processing Systems*, 36:10184–10196, 2023.
- [44] Juzhe Zhang, Jingyan Zhang, Zining Song, Zhanhe Shi, Chengfeng Zhao, Ye Shi, Jingyi Yu, Lan Xu, and Jingya Wang. Hoi-m³: Capture multiple humans and objects interaction within contextual environment. In *Proceedings of the IEEE/CVF Conference on Computer Vision and Pattern Recognition*, pages 516–526, 2024.
- [45] Zan Wang, Yixin Chen, Tengyu Liu, Yixin Zhu, Wei Liang, and Siyuan Huang. Humanise: Language-conditioned human motion generation in 3d scenes. *Advances in Neural Information Processing Systems*, 35:14959–14971, 2022.
- [46] Sangyun Shin, Kaichen Zhou, Madhu Vankadari, Andrew Markham, and Niki Trigoni. Spherical mask: Coarse-to-fine 3d point cloud instance segmentation with spherical representation. In *Proceedings of the IEEE/CVF Conference on Computer Vision and Pattern Recognition*, pages 4060–4069, 2024.